Finite Curvature and Corrugations in Dielectric Ridge Waveguides

T. ROZZI, SENIOR MEMBER, IEEE, GRAZIANO CERRI, FRANCO CHIARALUCE, ROBERTO DE LEO, AND RICHARD F. ORMONDROYD

Abstract—**Dielectric ridge waveguide is now widely used in passive and active integrated optics, and it could find use in millimeter-wave circuits. Families of devices such as ring lasers and couplers require structures with bends of finite length and relatively high curvature. The paper presents a technique, based on the concept of local modes, which also takes into account the corrugations due to fabrication. Results are in good qualitative agreement with experimental values reported in the literature.**

I. INTRODUCTION

DIELECTRIC RIDGE waveguides are now commonly used in integrated optics and millimeter-wave technology in order to achieve lateral guidance. The effective dielectric constant (EDC) solution to this type of problem was first presented in [1] and [2]. This method is in fact very accurate for most practical purposes. A rigorous solution to this problem by means of the transverse resonance diffraction (TRD) approach is discussed in [3]; a full treatment by a substantially similar approach is also given in [4].

With a view to integrating components and subsystems, curved structures are extremely important for a variety of reasons. The first is to reduce the area of material, and therefore costs, but also to realize coupling regions and resonators as well as to perform useful functions such as mode stripping.

The infinite bend in an infinite dielectric slab and fiber has received much attention in the literature from 1969 onwards [5], [6]; the reader is referred to existing textbooks such as [7] for extensive references.

Finite, relatively sharp bends, however, are required in integrated optics and especially short millimeter waves, where the end effects play a more important role. These are less well documented. An approach valid for paraxial rays is described in [8], for instance. In particular, the problem of propagation of a surface wave over a bend of a finitely conducting surface is treated in [9] by means of the "local modes" approach, of which more will be said in the following.

Manuscript received February 2, 1987; revised July 31, 1987. This work was supported in part by the EEC under the Laboratory Twinning Program, STI-079-JC(CD)

T. Rozzi and R. F. Ormondroyd are with the School of Electrical Engineering, University of Bath, Bath, England BA2 7AY.

G. Cerri, F. Chiaraluce, and R. De Leo are with the University of Ancona, Itaqly.

IEEE Log Number 8717902.

Much less is known about problems of bend in a ridge waveguide, finite and infinite. A theoretical treatment of the ring in a rib waveguide is found in [10], and the only experimental data known to us in the literature on a finite curve in a dielectric ridge waveguide seem to be those of [11]. Also interesting are the results of [12] on the germane problem of an image line bend and the theoretical treatment with experimental verification on the nonradiative waveguide given in [13]. In [11], the phenomenon of "anomalous bending losses" in the optical dielectric ridge waveguide is reported. This consists in the appearance of a minimum in the loss versus radius of curvature (R) characteristics in a curve guide of finite length.

It was surmised then that the presence of vertical corrugations of regular pitch and depth on the side walls of the ridge are at the origin of this effect. These corrugations arise from the fabrication process of the waveguides, and as such their occurrence can be controlled to a certain extent.

It is well known that the losses by curvature decrease roughly exponentially with the radius of curvature and therefore with the actual length of a bend of a given angle. The corrugations perturb the guided field, causing it to couple weakly to the radiation spectrum, an effect that increases with the length of the guide.

In this contribution we analyze the combined effect of finite curvature and corrugation in the dielectric ridge waveguide and conclude that the occurrence of the minimum is due to the balance of the two opposite effects over a fairly broad region of R/λ_0. Numerical results, including just these two contrasting effects, are in fact in agreement with the experimental results of [11], well within the scope of experimental and dimensional uncertainties.

In view of application to passive integrated optics and millimetrics (e.g., GaAs waveguides on a substrate of GaAlAs), the waveguide aspect ratio is such that the guided modes can be considered as LSE or LSM rather than full hybrid. On a straight section of guide, these two polarizations are not coupled. The presence of the bend, however, does cause some coupling to occur for relatively small values of R/λ_0, depending upon aspect ratio. This coupling effect is treated in [17] and is not considered here; i.e., we retain only the LSE case. This simplification considerably reduces the details of the analysis and highlights the essence of the method.

0018-9480/88/0100-0068$01.00 ©1988 IEEE

The effect of curvature is studied by means of a generalization of the "local modes" technique of [9]. In its principal form, this approach involves developing the transverse field (or potential) and its derivative along the axis of the bend at a given section in terms of the set of discrete and continuous modes of a straight waveguide of the same cross section as the curved one. Obviously this set varies along the bend in general, if the material parameters and/or the radius of curvature vary, which makes the technique very flexible indeed.

In its original form, however, the method is not well suited to handling the problem of radiation except over a very narrow paraxial beam, and serious convergence problems arise. We have studied in some depth the generalization of the technique, exploring two alternative solutions. As a result, we present in Section IV a semianalytical, iterative approach that is easy to implement on the computer and features excellent convergence under very general conditions.

The effect of corrugations is studied by means of a field-matching technique. The corrugation is modeled as a step discontinuity [14], [15], and by imposing the continuity of the tangential field, expressed in terms of discrete and continuous spectrum, at the transition between two contiguous sections, a transmission coefficient for the propagating waves can be obtained. As a result, the behavior of the EM field along the bend is described by a small system of integrodifferential equations (typically one or two), which is solved in conjunction with the field matching to take into account the corrugation.

In fact, the technique presented here is of much wider application in the microwave and millimeter-wave range, for instance, to the situation where discrete step discontinuities are deliberately inserted in a bend as matching elements or impedance transformers.

II. Modes of the Ridge Waveguide

The spectrum of the ridge waveguide can be described in terms of the LSE/LSM mode families, derivable from y-directed Hertzian potentials. Restricting ourselves to the LSE case, in view of the aspect ratio of the ridge, the field components are given by

$$E_x = \omega\mu\beta\Pi \tag{1a}$$

$$E_y = 0 \tag{1b}$$

$$E_z = -j\omega\mu\partial_x\Pi \tag{1c}$$

$$H_x = \partial^2_{xy}\Pi \tag{1d}$$

$$H_y = \beta^2\Pi - \partial^2_x\Pi \tag{1e}$$

$$H_z = -j\beta\partial_y\Pi \tag{1f}$$

where Π is the Hertzian potential ($\Pi = \Pi \boldsymbol{a}_y$) and the appropriate boundary conditions are imposed. The EDC is defined in each region of Fig. 1:

$$\epsilon_e^{\mathrm{I(II)}} = \epsilon_r^{\mathrm{I(II)}} - \left[\frac{k_y^{\mathrm{I(II)}}}{k_0}\right]^2. \tag{2}$$

By use of the EDC technique, equations (1) reduce to a simplified TM form and the detailed expression for field components, normalization, and continuous spectrum are given in Appendix I.

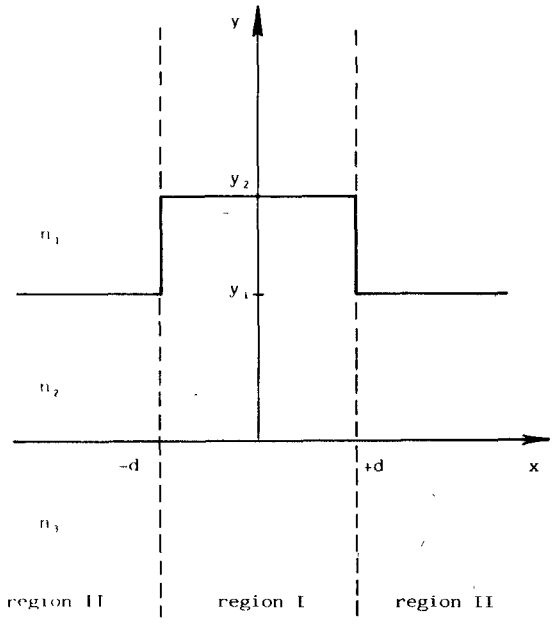

Fig. 1. Cross section of a ridge waveguide.

III. The Bend Problem

By means of the EDC technique, the 3-D problem of the bend in Fig. 2 has been reduced to a 2-D one, as shown in Fig. 3, where the geometry of the bend is also defined.

It is now important to introduce the concept of "local modes" [9] at an arbitrary cross section $z = z_0$. These are defined as the eigenfunctions of a straight guide whose cross section is the same as that of the curved guide at $z = z_0$. As such, they are solutions of the wave equation

$$\partial_x^2\psi_n + (\epsilon_e k_0^2 - \beta_n^2)\psi_n = 0 \tag{3}$$

in each piecewise homogeneous region and where it is explicitly noted that

$$\epsilon_e = \epsilon_e(z) \tag{4a}$$

$$\psi_n = \psi_n(x, z). \tag{4b}$$

However, if the radius R is assumed constant, and ϵ_e is also constant, then ψ_n is also constant with z.

The more general form above is useful in cases where the geometry loss (or gain) of the guide is not uniform in z. Let ϕ denote a scalar component of the global field. In our (TM) case it represents the magnetic H_y component (E_y in the TE case); both the latter and its z derivative can be expanded in terms of the ψ_n as

$$\phi = \sum_{\nu=-N}^{N} C_\nu\psi_\nu + \sum_{\mu=\pm}\int_0^\infty C_\mu(\chi)\psi(\chi)\,d\chi \tag{5}$$

$$\frac{d\phi}{dz} = -j\sum_{\nu=-N}^{N}\beta_\nu C_\nu\psi_\nu - j\sum_{\mu=\pm}\int_0^\infty \beta_\mu(\chi)C_\mu(\chi)\psi(\chi)\,d\chi \tag{6}$$

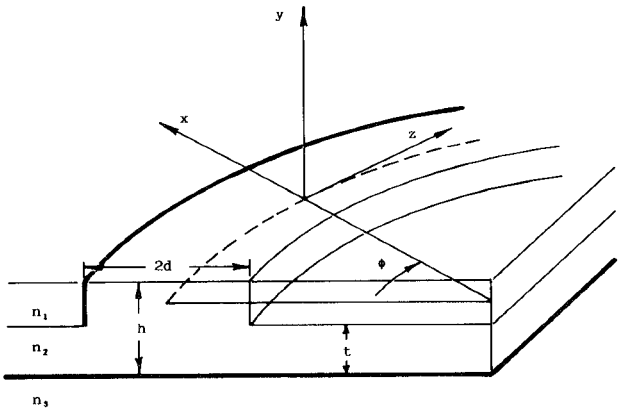

Fig 2. Geometry of a curved ridge waveguide.

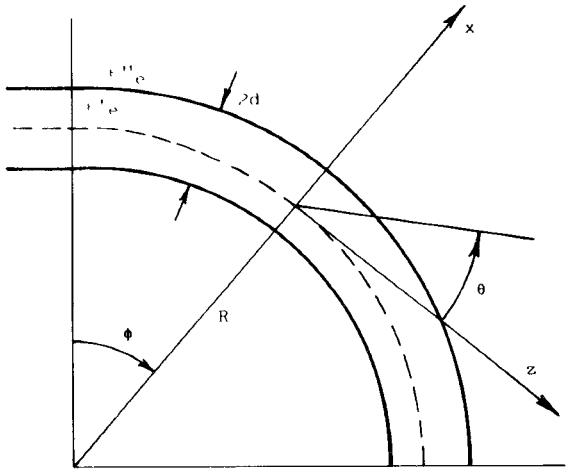

Fig 3 Equivalent bidimensional structure after using EDC.

where χ denotes the continuous index, and ν and $\mu \gtrless 0$ denote waves traveling in the positive and negative z direction, respectively. C_ν, $C_\mu(\chi)$ are the unknown amplitudes of the "local modes" $\psi_\nu e\psi(\chi)$, respectively. Equation (5) follows directly from completeness; (6) is an important consequence of the property of the modes to be local solutions of the wave equation.

Equating identically the z derivative of (5) to (6) and using the wave equation for ϕ, the following system of integrodifferential equations results:

$$D_n' = \sum_{\nu=-N}^{N} S_{n\nu} D_\nu e^{j(\gamma_n - \gamma_\nu)} + \sum_{\mu=\pm} \int_0^\infty S_{n\mu}(\chi) D_\mu(\chi) e^{j(\gamma_n - \beta_\mu(\chi)R\phi)} d\chi \qquad n = -N \cdots +N \quad (7)$$

$$D_m'(\sigma) = \sum_{\nu=-N}^{N} S_{\nu m}'(\sigma) D_\nu e^{j(\beta_m(\sigma)R\phi - \gamma_\nu)} + \sum_{\mu=\pm} \int_0^\infty S_\mu(\sigma,\chi) D_\mu(\chi) e^{jR\phi(\beta_m(\sigma) - \beta_\mu(\chi))} d\chi, \qquad m = \pm \quad (8)$$

where $S_{n\nu}$ denotes the coupling coefficient between two discrete modes, $S_{n\mu}$ and $S_{\nu m}'$ between a discrete mode and a continuous component, and $S_\mu(\sigma,\chi)$ between two continuous components. The D's are obtained from the amplitudes of the C's defined in (5) and (6) by conveniently collecting the "fast" phase variation, i.e.,

$$C_n(\phi) = D_n(\phi) e^{-j\gamma_n} \quad (9)$$

$$C_\mu(\phi,\chi) = D_\mu(\phi,\chi) e^{-j\beta_\mu(\chi)R\phi} \quad (10)$$

where

$$\gamma_n = \int_0^z \beta_n\, dz' = R\int_0^\phi \beta_n\, d\phi, \quad (11)$$

$$\beta_n^2(\chi) = \epsilon_2 k_0^2 + \chi^2 \qquad \beta_n = -\beta_n. \quad (12)$$

Details are given in Appendix II.

IV. Solution of the Integrodifferential Equations

The system of equations comprising (7) and (8) is integrodifferential of the first order and in principle it can be solved by various techniques. The difficulty consists in the fact that (8) depends on a continuous index χ and, as such, corresponds to a continuous infinity of equations. It may be useful to consider briefly the approaches that were attempted.

In [9] the method of discrete sampling over the anges of radiation was originally proposed. In practice, it is found that the resulting large system of discrete equations is numerically unstable for all but a small number of sampling angles, ideally centered around a paraxial beam. We also tried the method of a discrete integral transform of the continuous spectrum by means of weighted Laguerre functions, as originally described in [16] for application to discontinuity problems. While numerically more stable than the preceding one, this approach also shows poor convergence in the case of small differences of refractive indices.

The approach we eventually followed, with satisfactory results under all conditions, is the contraction and iterative solution of the system, as described below.

The following nonessential simplifications are now introduced for the sake of clarity.

a) We consider a single guided mode.
b) Reflected waves are neglected for both the discrete and continuous spectrum.

Moreover, the following essential simplification is physically well justified, namely, that the weak coupling of the continuum to itself is neglected.

The system comprising (7) and (8) is then reduced to

$$D_1'(\phi) = \int_0^\infty S_1(\chi) D(\chi,\phi) e^{-jR[\beta(\chi) - \beta_1]\phi} d\chi \quad (13)$$

$$D'(\chi,\phi) = S_{+o}'(\chi) D_1(\phi) e^{-jR[\beta_1 - \beta(\chi)]\phi}. \quad (14)$$

The index o (odd) has been introduced in order to point out that the fundamental even mode excites the odd components of the continuum spectrum only.

We integrate the second equation above, obtaining

$$D(\chi,\phi) = \int_{\phi_0}^{\phi} S'_{+o}(\chi) D_1(\zeta) e^{-jR[\beta_1-\beta(\chi)]\zeta}\, d\zeta + D(\chi,\phi_0) \tag{15}$$

where ϕ_0 denotes an initial angle, which we normally assume to be zero, with $D(\chi,0)=0$. We are now in a position to substitute (15) into (13), obtaining an integro-differential equation for the guided mode only:

$$D_1'(\phi) = \int_0^{\infty} S_{+o}(\chi)\left[\int_0^{\phi} D_1(\zeta) e^{-jR[\beta_1-\beta(\chi)]\zeta}\, d\zeta\right] \cdot e^{-jR[\beta(\chi)-\beta_1]\phi} d\chi. \tag{16}$$

The integral over ζ in the angle interval $0 \leqslant \zeta \leqslant \phi$ is carried out in a convenient, semianalytical iterative manner. This is done by dividing the interval into N equal subintervals of width $\Delta\phi$, so that $\phi = N\Delta\phi$, and assuming the following linearization of the unknown amplitude D_1 over each interval n $(1 < n < N)$:

$$D_{1n}(\zeta) = a_n + b_n[\zeta - (n-1)\Delta\phi]. \tag{17}$$

In particular, we have

$$D'_{1n}(n\Delta\phi) = b_n. \tag{18}$$

Owing to the above linearization, we obtain from (16)

$$b_n = \int_0^{\infty} S_{+o}(\chi) S'_{+o}(\chi) \cdot\left[\sum_{m=1}^{n} \int_{(m-1)\Delta\phi}^{m\Delta\phi} [a_m + b_m(\zeta-(n-1)\Delta\phi)] \cdot e^{-jR[\beta_1-\beta(\chi)]\zeta}\, d\zeta\right] e^{-jR[\beta(\chi)-\beta_1]n\Delta\phi} d\chi. \tag{19}$$

Equation (19) now lends itself to simple quadrature, leading, finally, to an iterative expression that links the coefficients a_n, b_n:

$$b_n = \left\{ a_n I_0 - a_1 I_n + \sum_{m=1}^{n-1} [b_m(J_{n-m} - J_{n+1-m})] \right\} \cdot /\{1 - \Delta\phi I_0 - [J_0 - J_1]\} \tag{20}$$

where $a_1 = 1$ is the initial amplitude of the guided mode, and the expressions for J_n and I_n are reported in Appendix III together with the detailed derivation of (20) from (19). For a smooth curve, the linearization (17) can be further simplified:

$$a_{n+1} = b_n \Delta\phi + a_n. \tag{21}$$

The above, together with (20) and the initial condition $a_1 = 1$, is sufficient to determine all the amplitudes a_n, b_n.

In the presence of corrugation, however, a_n becomes discontinuous at each change of width as

$$a_{n+1} = T(b_n \Delta\phi + a_n) \tag{22}$$

where T is the transmission coefficient from a section to the next to be determined in the following.

It is noted that the above procedure lends itself to easy numerical evaluation and is stable with respect to the variation of geometrical and material parameters.

V. The Effect of Corrugation

As mentioned in the Introduction, the fabrication process of ridge waveguide creates a vertical corrugation on the side walls of the ridge, as shown in Fig. 4. Again by use of the EDC technique, one is reduced to the equivalent structure of Fig. 5, which illustrates the geometry under consideration.

The pitch of the corrugation normalized to wavelengths is such that it is possible to identify the angle interval $\Delta\phi$ employed in the integration of Section IV with the angular interval corresponding to the pitch over the radius of curvature, i.e., the angle that corresponds to a single corrugation, though this identification is not essential. The corrugation depth is roughly the same as the pitch, so that it can be considered as a small step discontinuity, i.e., such that reflected waves can be neglected, again, a nonessential simplification. With reference to Fig. 6, let us consider a discontinuity at $z = z_0$ in passing from a section of width $2d$ to one of width $2D$; the tangential field in $z = z_0$ and in $z = z_0^+$, can be expressed as

$$\phi|_{z=z_0^-} = C_1(z_0^-)\psi_{1l}(x) + \int_0^{\infty} C^e(z_0^-,\chi)\psi_l^e(\chi,x)\, d\chi + \int_0^{\infty} C^o(z_0^-,\chi)\psi_l^o(\chi,x)\, d\chi \tag{23}$$

$$\phi|_{z=z_0^+} = C_1(z_0^+)\psi_{1r}(x) + \int_0^{\infty} C^e(z_0^+,\chi)\psi_r^e(\chi,x)\, d\chi + \int_0^{\infty} C^o(z_0^+,\chi)\psi_r^o(\chi,x)\, d\chi \tag{24}$$

where the superscript e means even and o means odd, so that $\psi_l^e(\chi,x)$, $\psi_l^o(\chi,x)$, $\psi_r^e(\chi,x)$, $\psi_r^o(\chi,x)$ represent the even and odd continuous components on the left (l) and the right (r) of the transition respectively, and ψ_{1l}, ψ_{1r} denote the corresponding discrete modes at the two sides of the discontinuity.

By imposing continuity of the tangential field in $z = z_0$, and using the orthonormality properties of the modes, it is possible to write the expressions for the amplitude of the "local modes":

$$C_1(z_0^+) \cong C_1(z_0^-)\left\langle \frac{\psi_{1l}\psi_{1r}}{\epsilon} \right\rangle + \int_0^{\infty} C^e(z_0^-,\chi)\left\langle \frac{\psi_l^e(\chi)\psi_{1r}}{\epsilon} \right\rangle d\chi \tag{25}$$

$$C^e(z_0^+,\chi) \cong C_1(z_0^-)\left\langle \frac{\psi_{1l}\psi_r^e(\chi)}{\epsilon} \right\rangle + C^e(z_0^-,\chi) \tag{26}$$

$$C^o(z_0^+,\chi) \cong C^o(z_0^-,\chi) \tag{27}$$

where the bracket symbol $\langle \cdots \rangle$ denotes integration in the range $-\infty < x < +\infty$.

It is noted that in the application considered here, the amplitude of the (even) continuum excited by the discontinuity is at least three orders of magnitude smaller than that of the guided mode. It is permissible therefore to neglect the interaction via the continuum between successive steps.

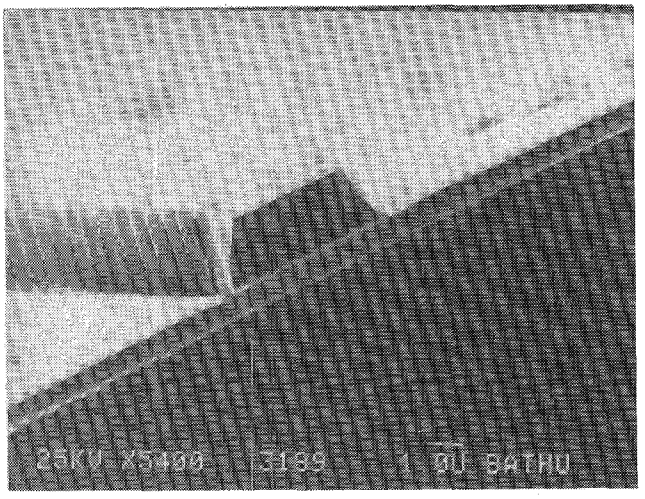

Fig. 4. Photograph showing edge corrugations of a ridge waveguide.

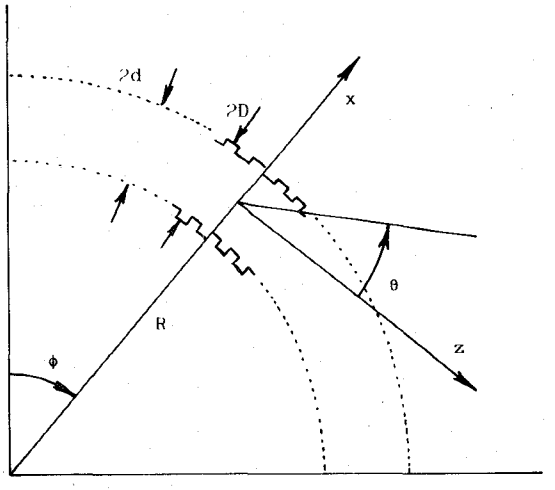

Fig. 5. Equivalent bidimensional structure of a curved waveguide with edge roughness.

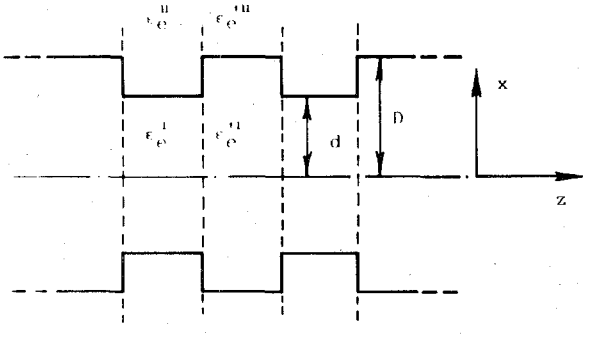

Fig. 6. Corrugations as step discontinuities.

The transmission coefficient of the transition between two contiguous piecewise uniform sections for the fundamental mode is therefore given by

$$T = \left\langle \frac{\psi_{1l}\psi_{1r}}{\epsilon} \right\rangle \tag{28}$$

This transmission coefficient is required in (22), which is then employed together with (20) in order to find all the values of a_n, b_n iteratively for a corrugated guide.

VI. Extension to Overmoded Waveguide

With a procedure quite similar to the one described in Section IV, the iterative method can be extended to a waveguide which can support two or more modes. Let us consider, in particular, the bimodal case, where the fundamental (even) mode and first higher order (odd) mode are propagating. Under the hypothesis of negligible coupling between the continuous components of the spectrum, the differential equations for the odd continuum, excited by the fundamental mode, and the even continuum, excited by the second mode, can be eliminated analytically, in a manner analogous to that described in Section IV.

After substitution, two coupled differential equations for the surface waves, analogous to (16), are obtained. An appropriate linearization, of the same kind as in (17), for the unknown amplitudes D_1 and D_2 over each interval is introduced, leading to a system of linear equations which generalizes (19).

The final iterative expression corresponding to (20) has the following matrix structure:

$$\begin{bmatrix} E_n^{11} & E_n^{12} \\ E_n^{21} & E_n^{22} \end{bmatrix} \begin{bmatrix} b_n^1 \\ b_n^2 \end{bmatrix} = \begin{bmatrix} P_n^1 \\ P_n^2 \end{bmatrix} \tag{29}$$

where

$$E_n^{11} = E_n^{22} = 1 \tag{30a}$$

$$E_n^{12} = -\Delta\phi \frac{S_{12}}{B^1} e^{-j(\beta_1-\beta_1)Rn\Delta\phi} \tag{30b}$$

$$E_n^{21} = -\Delta\phi \frac{S_{21}}{B^2} e^{-j(\beta_1-\beta_2)Rn\Delta\phi} \tag{30c}$$

$$P_n^1 = \frac{S_{12}}{B^1} a_n^2 e^{-j(\beta_2-\beta_1)Rn\Delta\phi} + \frac{A_n^1}{B^1} \tag{30d}$$

$$P_n^2 = \frac{S_{21}}{B^2} a_n^1 e^{-j(\beta_1-\beta_2)Rn\Delta\phi} + \frac{A_n^2}{B^2} \tag{30e}$$

with

$$A_n^k = a_n^k I_0^k - a_1^k I_n^k + \sum_{i=1}^{n-1} b_i^k \left(J_{n-i}^k - J_{n-i+1}^k \right) \tag{30f}$$

$$B^k = 1 - \Delta\phi I_0^k - \left(J_0^k - J_1^k \right), \qquad k = 1,2 \tag{30g}$$

where the indices 1 and 2 refer to the corresponding modes.

Equation (29) has to be used in conjunction with the following one, describing the effect of the step discontinuity:

$$\begin{bmatrix} a_{n+1}^1 \\ a_{n+1}^2 \end{bmatrix} = \begin{bmatrix} T^1 & 0 \\ 0 & T^2 \end{bmatrix} \left[\begin{bmatrix} b_n^1 \\ b_n^2 \end{bmatrix} \Delta\phi + \begin{bmatrix} a_n^1 \\ a_n^2 \end{bmatrix} \right] \tag{31}$$

and the initial condition $a_1^1 = 1, a_1^2 = 0$.

All the elements I_n^1, J_n^1 are reported in Appendix III, T^1 has the form (28). The elements I_n^2, J_n^2, T^2 are obtained from the ones relative to the first mode replacing the corresponding parameters of the second mode and the odd continuous spectrum with the even continuous spectrum.

VII. Results

A computer program has been developed in order to analyze the corrugated curved ridge waveguide. The following parameters were assumed in the calculations:

$$n_1 = 1$$
$$n_2 = 3.44$$
$$n_3 = 3.4$$
$$t = 0.6\ \mu\text{m}$$
$$h = 1\ \mu\text{m}$$
$$2d = 1.5\ \mu\text{m}.$$

Both the depth and the width of the corrugations were taken as 100 nm, for a 90° bend. The resulting waveguide, for $\lambda_0 = 1.15\ \mu$m, is monomode.

In Fig. 7, the behavior of the field along the bend is shown for structures with radius of curvature $R = 50\lambda_0$, without and with material losses (attenuation coefficient $2\beta'' = 4.8\ \text{cm}^{-1}$) and without and with corrugations. It is noticeable how, for a short arc length, the effect of corrugation is negligible; oscillations of the amplitude of the fundamental mode are due to a back coupling of the continuous spectrum with the guided mode itself: this phenomenon is quite evident if the material is ideal, while even small losses prevent energy from going back into the guide.

The effect of material losses is now examined: a small negative imaginary part of the same magnitude was introduced in both n_2 and n_3 to give a prescribed imaginary part of the propagation constant of the surface wave along the z direction ($\beta = \beta' - j\beta''$); $2\beta'' = 0, 2, 4.8, 8\ \text{cm}^{-1}$.

The amplitude of the fundamental mode for a $R = 50\lambda_0$ guide is reported in Fig. 8 for the above values of β''.

The amplitude of the guided mode in a material with low losses ($2\beta'' = 4.8\ \text{cm}^{-1}$) is given for bends of various radii of curvature, neglecting corrugations (Fig. 9) and considering corrugations (Fig. 10). As previously mentioned, as the radius R increases, the effect of corrugations is increasingly noticeable.

In Fig. 11 the radiation pattern at the onset of the bend shows the preferential angles of radiation from which energy is lost: angles are considered from the tangent to the guide.

In order to make a comparison with experimental data, a ridge waveguide with the following characteristics was analyzed:

$$n_1 = 1$$
$$n_2 = 3.44$$
$$n_3 = 3.35$$
$$t = 0.4\ \mu\text{m}$$
$$h = 0.8\ \mu\text{m}$$
$$2d = 3\ \mu\text{m}.$$

The depth and the width of corrugations were assumed to be 70 and 100 nm, respectively, which is of the right order of magnitude of the actual geometry. A small negative imaginary part was introduced in n_2, n_3 in order to get an attenuation coefficient $2\beta'' = 6.9\ \text{cm}^{-1}$, for $\lambda_0 = 1.15\ \mu$m. Such was the structure experimentally investigated in [11]. With these dimensions, the guide supports in fact three LSE modes, the (even) fundamental, the (odd) first higher order mode, and the (even) second higher order mode. As the latter does not couple directly to the fundamental mode, the effect of its presence is negligible.

With respect to the monomode guide, a different loss mechanism for the fundamental mode (the only one present at the beginning of the curve) can be observed. In the

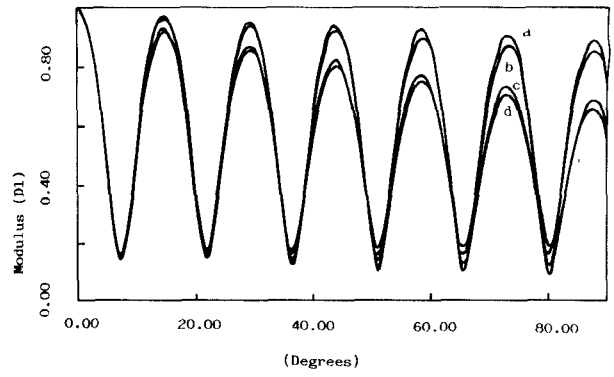

Fig. 7. Amplitude of the field versus arc length for a bend with $R = 50\lambda_0$. Without material losses and (a) without and (b) with corrugations. With material losses and (c) without and (d) with corrugations.

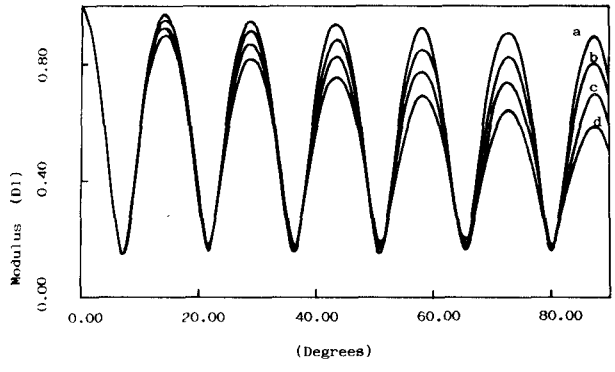

Fig. 8. Amplitude of the field versus arc length for a $R = 50\lambda_0$ and different material losses: (a) $\beta'' = 0$. (b) $\beta'' = 2$. (c) $\beta'' = 4.8$. (d) $\beta'' = 8$ β'' in cm^{-1}.

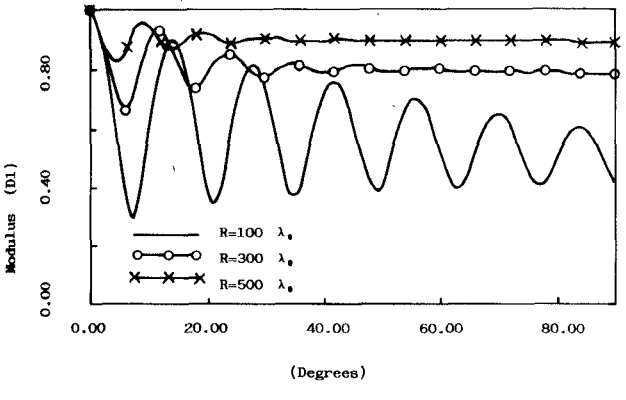

Fig. 9. Amplitude of the field versus arc length for bends with various radii of curvature without corrugation.

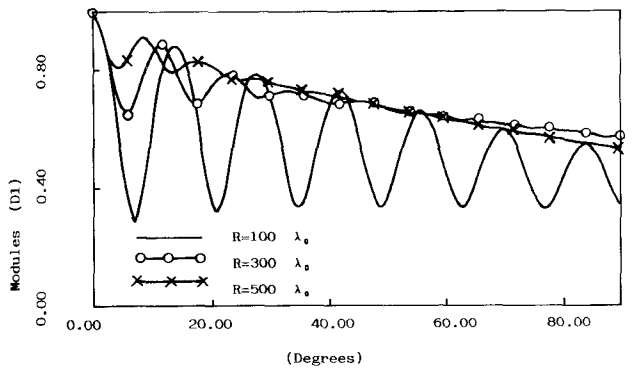

Fig. 10. Amplitude of the field versus arc length for bends with various radii of curvature with corrugation.

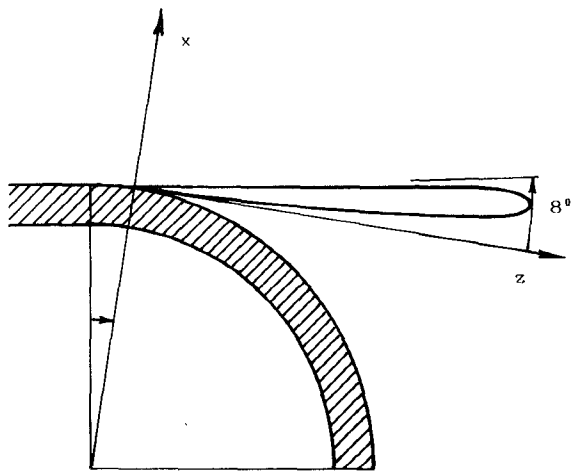

Fig 11 Radiation pattern at onset of bend.

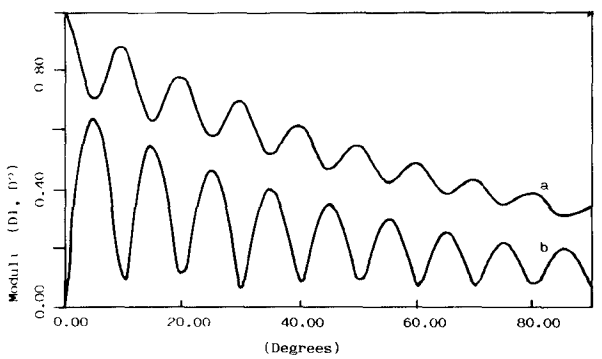

Fig. 12. Amplitudes of (a) the fundamental and (b) the first higher mode for a corrugated bend with $R = 400\lambda_0$.

previous case, in fact, bending losses were due entirely to the strong coupling between the surface wave and the (odd) continuum. In this case, however, the stronger coupling between the fundamental mode and the first higher order (coupled by curvature), as well as the coupling between the first higher order and the (even) continuum, dominates.

In Fig. 12 this effect is shown: the moduli of the fundamental and first higher modes are plotted as a function of the arc for a corrugated bend with $R = 400\lambda_0$.

In Fig. 13 the losses versus radius of curvature are finally reported for various values of the depth of corrugation, $2(D - d)$. In particular, curve e refers to the structure without corrugations and f gives the losses due to radiation only (no corrugations, no material losses). Dots represent experimental data inferred from [11] after subtracting the remaining overall experimental losses (i.e., input and output coupling), these were estimated at -11.5 dB, but their actual magnitude is uncertain. Also uncertain are the pitch and the depth of corrugation of the actual structure. A minimum value of the losses corresponding to an optimum radius of curvature can be noted when the effects of curvature and corrugations are balanced.

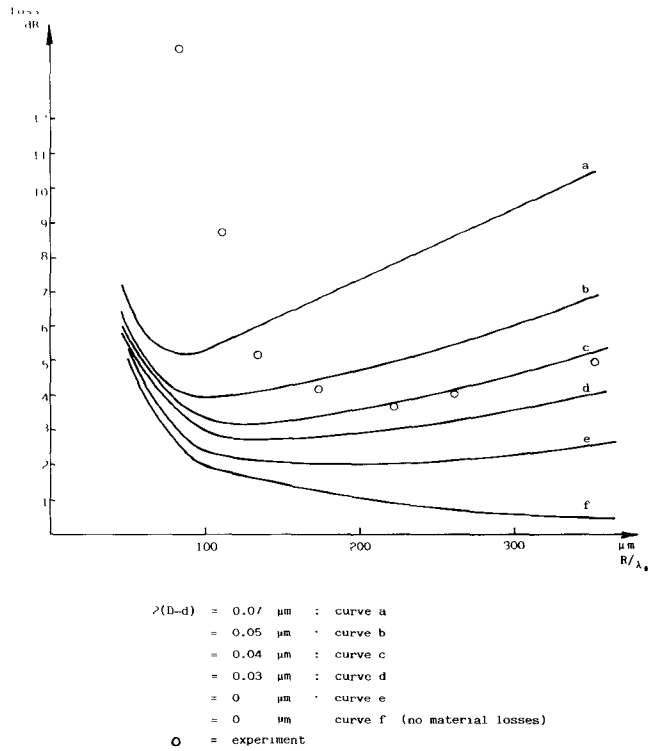

Fig. 13. Losses as a function of radius of curvature: numerical results for waveguides (a) without and (b) with corrugations. Dots represent experimental data from [11].

VIII. Conclusions

We present a development of the "local modes" technique which is capable of handling finite, tight bends in open dielectric waveguides of the LSE—LSM type, together with step discontinuities along the arc. By analytical manipulation of the continuum, the approach results in a small system of coupled integrodifferential equations, one for each discrete propagating mode. The latter system is solved analytically by means of an iterative approach to the point where it can be implemented on a desktop computer.

The method was applied to the curved, corrugated, dielectric ridge waveguide, yielding numerical results in general agreement with published experimental points. The technique is equally applicable to other curved open transmission media in the microwave, millimetric, and integrated optics ranges.

APPENDIX I

A. Surface Waves

If regions I and II in Fig. 1 are taken to be infinitely long in the x direction ($\partial_x = 0$), we have two layered asymmetric slab waveguides, and the field components are given by

$$E_x^{\mathrm{I(II)}} = \phi^{\mathrm{I(II)}}(y) \tag{A1a}$$

$$H_y^{\mathrm{I(II)}} = \frac{\beta}{\omega\mu}\phi^{\mathrm{I(II)}}(y) \tag{A1b}$$

$$H_z^{\mathrm{I(II)}} = \frac{-j}{\omega\mu}\partial_y \Phi^{\mathrm{I(II)}}(y) \tag{A1c}$$

where

$$\phi^{\mathrm{I(II)}}(y) = \begin{cases} A_c^{\mathrm{I(II)}}\cos\left(k_y^{\mathrm{I(II)}}y\right) + A_s^{\mathrm{I(II)}}\sin\left(k_y^{\mathrm{I(II)}}y\right), \\ \qquad 0 \leqslant y \leqslant y_{1(2)} & \text{(A2a)} \\ B^{\mathrm{I(II)}}e^{-\gamma_1^{\mathrm{I(II)}}(y - y_{2(1)})}, \qquad y \geqslant y_{1(2)} & \text{(A2b)} \\ C^{\mathrm{I(II)}}e^{+\gamma_3^{\mathrm{I(II)}}y}, \qquad y \leqslant 0. & \text{(A2c)} \end{cases}$$

By applying the boundary conditions for E_x and H_z, the eigenvalue equations for even TE and odd modes are obtained, and from the wave equation, the conservation of wavenumber results:

$$\epsilon_e^{\mathrm{I(II)}}k_0^2 = \epsilon_2 k_0^2 - k_y^{2\mathrm{I(II)}} = \gamma_1^{2\mathrm{I(II)}} + \epsilon_1 k_0^2 = \gamma_3^{2\mathrm{I(II)}} + \epsilon_3 k_0^2. \tag{A3}$$

In order to analyze the x variation ($\partial_y = 0$) using the concept of EDC, we consider the following fields:

$$E_x = \frac{\beta}{\epsilon_e \omega \epsilon_0}\Psi(x) \tag{A4a}$$

$$E_z = \frac{-j}{\epsilon_e \omega \epsilon_0}\partial_x \Psi(x) \tag{A4b}$$

$$H_y = \Psi(x) \tag{A4c}$$

where

$$\Psi(x) = \begin{cases} A^e\cos(k_x\gamma_x), & |x| \leqslant d \\ A^e\cos(k_x d)e^{-\gamma_x|x-d|}, & |x| \geqslant d \end{cases} \tag{A5a}$$

for even modes, and

$$\Psi(x) = \begin{cases} A^o\sin(k_x x), & |x| \leqslant d \\ \dfrac{|x|}{x}A^o\sin(k_x d)e^{-\gamma_x|x-d|}, & |x| \geqslant d \end{cases} \tag{A5b}$$

for odd modes.

Boundary conditions for E_z give the eigenvalue equations for TM even and odd modes, which, in conjunction with the following expressions, obtained from the wave equation

$$\beta^2 = \epsilon_e^{\mathrm{I}}k_0^2 - k_x^2 = \epsilon_e^{\mathrm{II}}k_0^2 + \gamma_x^2 \tag{A6}$$

allow the determination of propagation constants and field configuration for the surface waves.

The normalization constant $A^{e(o)}$ is evaluated by the requirement

$$\int_{-\infty}^{+\infty}\frac{\Psi^2(x)}{\epsilon_e(x)}dx = 1 \tag{A7}$$

to be

$$A^{e(o)} = \sqrt{\frac{\epsilon_e^{\mathrm{I}}}{d + \dfrac{\epsilon_3^{\mathrm{I}}}{\epsilon_e^{\mathrm{II}}}\cdot\dfrac{1}{\gamma_x} \pm \dfrac{\sin(k_x d)\cos(k_x d)}{k_x}\left[1 - \left[\dfrac{\epsilon_3^{\mathrm{I}}}{\epsilon_e^{\mathrm{II}}}\right]^2\right]}} \tag{A8}$$

where the sign + is for even modes and sign − is for odd modes.

B. Continuous Spectrum

The continuous spectrum, together with the surface waves, constitutes a complete representation of the field in the slab. H_y is given by $H_y = \Psi(\chi, x)$, where

$$\Psi^e(\chi, x) = \begin{cases} \sqrt{\dfrac{\epsilon_e^{\mathrm{II}}}{\pi}}\cos\left[\chi(x+d) - \alpha_e\right], \\ \qquad x \leqslant -d & \text{(A9a)} \\ \sqrt{\dfrac{\epsilon_e^{\mathrm{II}}}{\pi}}\dfrac{1}{C_e}\cos(sx), \\ \qquad -d \leqslant x \leqslant d & \text{(A9b)} \\ \sqrt{\dfrac{\epsilon_e^{\mathrm{II}}}{\pi}}\cos\left[\chi(x-d) + \alpha_e\right], \\ \qquad x \geqslant d & \text{(A9c)} \end{cases}$$

with

$$s^2 = \chi^2 + \left(\epsilon_e^{\mathrm{I}} - \epsilon_e^{\mathrm{II}}\right)k_0^2, \qquad 0 \leqslant \chi < \infty \tag{A10a}$$

$$C_e = \sqrt{\cos^2(sd) + \left[\frac{s\epsilon_e^{\mathrm{II}}}{\chi\epsilon_e^{\mathrm{I}}}\right]^2\sin^2(sd)} \tag{A10b}$$

$$\alpha_e = tg^{-1}\left[\left[\frac{s\epsilon_e^{\mathrm{II}}}{\chi\epsilon_e^{\mathrm{I}}}\right]tg(sd)\right] \tag{A10c}$$

for even TM components and

$$\Psi^o(\chi, x) = \begin{cases} -\sqrt{\dfrac{\epsilon_e^{\mathrm{II}}}{\pi}}\cos\left[\chi(x+d) + \alpha_o\right], \\ \qquad x \leqslant -d & \text{(A11a)} \\ \sqrt{\dfrac{\epsilon_e^{\mathrm{II}}}{\pi}}\dfrac{1}{C_o}\sin(sx), \\ \qquad -d \leqslant x \leqslant d & \text{(A11b)} \\ \sqrt{\dfrac{\epsilon_e^{\mathrm{II}}}{\pi}}\cos\left[\chi(x-d) - \alpha_o\right], \\ \qquad x \geqslant d & \text{(A11c)} \end{cases}$$

with

$$s^2 = \chi^2 + \left(\epsilon_e^{\mathrm{I}} - \epsilon_e^{\mathrm{II}}\right)k_0^2, \qquad 0 \leqslant \chi < \infty \tag{A12a}$$

$$C_o = \sqrt{\sin^2(sd) + \left[\frac{s\epsilon_e^{\mathrm{II}}}{\chi\epsilon_e^{\mathrm{I}}}\right]^2 \cos^2(sd)} \tag{A12b}$$

$$\alpha_o = tg^{-1}\left[\left[\frac{s\epsilon_e^{\mathrm{II}}}{\chi\epsilon_e^{\mathrm{I}}}\right]\mathrm{cotg}(sd)\right] \tag{A12c}$$

for odd TM components.

Appendix II

For the system of local coordinates of Fig. 2,

$$\partial_\rho = \partial_x \qquad \rho = R + x \qquad \frac{1}{\rho}\partial_\Phi = \partial_z \tag{A13}$$

the wave equation can be written as

$$\left[\partial_\rho^2 + \frac{1}{\rho}\partial_\rho + \frac{1}{\rho^2}\partial_\phi^2\right]\Phi + \epsilon_e k_0^2 \Phi = 0. \tag{A14}$$

After differentiating (5) with respect to z, equating it to (6), and recalling (A13),

$$\begin{aligned}
&\sum_{\nu=-N}^{N}(C_\nu' + jR\beta_\nu C_\nu)\psi_\nu \\
&\quad + \sum_{\mu=\pm}\int_0^\infty \left[C_\mu'(\chi) + jR\beta_\mu(\chi)C_\mu(\chi)\right]\psi(\chi)\,d\chi \\
&\quad = -j\sum_{\nu=-N}^{N}\beta_\nu C_\nu x\psi_\nu \\
&\quad\quad - j\sum_{\mu=\pm}\int_0^\infty \beta_\mu(\chi)C_\mu(\chi)x\psi(\chi)\,d\chi \\
&\quad\quad - \sum_{\nu=-N}^{N} C_\nu\psi_\nu' - \sum_{\mu=\pm}\int_0^\infty C_\mu(\chi)\psi'(\chi)\,d\chi
\end{aligned} \tag{A15}$$

where the prime indicates differentiation with respect to z.

Substituting (5) and (6) together in the wave equation (A14), yields

$$\begin{aligned}
&\sum_{\nu=-N}^{N}\left[\partial_\rho^2 + \frac{1}{\rho}\partial_\rho\right]C_\nu\psi_\nu \\
&\quad + \sum_{\mu=\pm}\int_0^\infty C_\mu(\chi)\left[\partial_\rho^2 + \frac{1}{\rho}\partial_\rho\right]\psi(\chi)\,d\chi \\
&\quad - \frac{j}{\rho}\left\{\sum_{\nu=-N}^{N}\partial_\phi(\beta_\nu C_\nu\psi_\nu)\right. \\
&\quad\quad \left. + \sum_{\mu=\pm}\int_0^\infty \partial_\phi\left[\beta_\mu(\chi)C_\mu(\chi)\psi(\chi)\right]d\chi\right\} \\
&\quad + \sum_{\nu=-N}^{N} C_\nu\epsilon_e k_0^2\psi_\nu + \sum_{\mu=\pm}\int_0^\infty C_\mu(\chi)\epsilon_e k_0^2\psi(\chi)\,d\chi = 0.
\end{aligned} \tag{A16}$$

By multiplying by $\rho = R + x$, carrying out the ψ differentiation explicitly, recalling (A13), and using (3), (A16) becomes

$$\begin{aligned}
&\sum_{\nu=-N}^{N} C_\nu\beta_\nu^2 R\psi_\nu + \sum_{\mu=\pm}\int_0^\infty C_\mu(\chi)\beta_\mu^2(\chi)R\psi(\chi)\,d\chi \\
&\quad - j\left\{\sum_{\nu=-N}^{N}(\beta_\nu' C_\nu\psi_\nu + \beta_\nu C_\nu'\psi_\nu + \beta_\nu C_\nu\psi_\nu')\right. \\
&\quad + \sum_{\mu=\pm}\int_0^\infty\left[\beta_\mu'(\chi)C_\mu(\chi)\psi(\chi) + \beta_\mu(\chi)C_\mu'(\chi)\psi(\chi)\right. \\
&\quad\quad \left.\left. + \beta_\mu(\chi)C_\mu(\chi)\psi'(\chi)\right]d\chi\right\} \\
&\quad + \sum_{\nu=-N}^{N} C_\nu\beta_\mu^2 x\psi_\nu + \sum_{\mu=\pm}\int_0^\infty C_\mu(\chi)\beta_\mu^2(\chi)x\psi(\chi)\,d\chi \\
&\quad + \sum_{\nu=-N}^{N} C_\nu\partial_x\psi_\nu + \sum_{\mu=\pm}\int_0^\infty C_\mu(\chi)\partial_x\psi(\chi)\,d\chi = 0.
\end{aligned} \tag{A17}$$

Multiplying (A15) by $\psi_n/\epsilon_e(x)$ and integrating and similarly for (A17), using the following orthonormality properties for "local modes":

$$\left\langle\frac{\psi_n\psi_\nu}{\epsilon_e}\right\rangle = \delta_{n|\nu|} \tag{A18a}$$

$$\left\langle\frac{\psi_n\psi(\chi)}{\epsilon_e}\right\rangle = 0 \tag{A18b}$$

$$\left\langle\frac{\psi(\chi)\psi(\sigma)}{\epsilon_e}\right\rangle = \delta(\chi - \sigma) \tag{A18c}$$

we obtain

$$\begin{aligned}
&\sum_{\nu=\pm n}(C_\nu' + jR\beta_\nu C_\nu) \\
&\quad = -j\sum_{\nu=-N}^{N}\beta_\nu C_\nu\left\langle\frac{\psi_n x\psi_\nu}{\epsilon_e}\right\rangle \\
&\quad\quad - j\sum_{\mu=\pm}\int_0^\infty \beta_\mu(\chi)C_\mu(\chi)\left\langle\frac{\psi_n x\psi(\chi)}{\epsilon_e}\right\rangle d\chi \\
&\quad\quad - \sum_{\nu=-N}^{N} C_\nu\left\langle\frac{\psi_n\psi_\nu'}{\epsilon_e}\right\rangle - \sum_{\mu=\pm}\int_0^\infty C_\mu(\chi)\left\langle\frac{\psi_n\psi'(\chi)}{\epsilon_e}\right\rangle d\chi
\end{aligned} \tag{A19a}$$

$$\begin{aligned}
&\sum_{\nu=\pm n}\pm(C_\nu' + j\beta_\nu C_\nu R) \\
&\quad = -\sum_{\nu=-N}^{N}\left[\frac{\beta_\nu'}{\beta_{|n|}}\delta_{|n|\nu} + \frac{\beta_\nu}{\beta_{|n|}}\left\langle\frac{\psi_n\psi_\nu'}{\epsilon_e}\right\rangle\right. \\
&\quad\quad \left. + j\frac{\beta_\nu^2}{\beta_{|n|}}\left\langle\frac{\psi_n x\psi_\nu}{\epsilon_e}\right\rangle + j\frac{1}{\beta_{|n|}}\left\langle\frac{\psi_n\partial_x\psi_\nu}{\epsilon_e}\right\rangle\right]C_\nu \\
&\quad\quad - \sum_{\mu=\pm}\int_0^\infty d\chi\left[\frac{\beta_\mu(\chi)}{\beta_{|n|}}\left\langle\frac{\psi_n\psi'(\chi)}{\epsilon_e}\right\rangle\right. \\
&\quad\quad\quad + j\frac{\beta_\mu^2(\chi)}{\beta_{|n|}}\left\langle\frac{\psi_n x\psi(\chi)}{\epsilon_e}\right\rangle \\
&\quad\quad\quad \left. + j\frac{1}{\beta_{|n|}}\left\langle\frac{\psi_n\partial_x\psi_\mu(\chi)}{\epsilon_e}\right\rangle\right]C_\mu(\chi)
\end{aligned} \tag{A19b}$$

Recalling that $\beta_{-\nu} = -\beta_\nu$, upon adding and subtracting (A19a) and (A19b) we obtain the integrodifferential equations for the amplitudes of the surface waves:

$$C_n' + j\beta_n R C_n = \sum_{\nu=-N}^{N} S_{n\nu} C_\nu + \sum_{\mu=\pm} \int_0^\infty S_{n\mu}(\chi) C_\mu(\chi)\, d\chi \tag{A20}$$

where $n = -N, \cdots, -1, 1, \cdots, N$ and

$$S_{n\nu} = -\frac{1}{2}\left[j\beta_\nu \left\langle \frac{\psi_n x \psi_\nu}{\epsilon_e} \right\rangle + \left\langle \frac{\psi_n \psi_\nu'}{\epsilon_e} \right\rangle \pm \frac{\beta_\nu'}{\beta_{|n|}} \delta_{n|\nu|} \pm \frac{\beta_\nu}{\beta_{|n|}} \left\langle \frac{\psi_n \psi_\nu'}{\epsilon_e} \right\rangle \pm j \frac{\beta_\nu^2}{\beta_{|n|}} \left\langle \frac{\psi_n x \psi_\nu}{\epsilon_e} \right\rangle \pm j \frac{1}{\beta_{|n|}} \left\langle \frac{\psi_n \partial_x \psi_\nu}{\epsilon_e} \right\rangle \right] \tag{A21a}$$

$$S_{n\mu}(\chi) = -\frac{1}{2}\left[j\beta_\mu(\chi) \left\langle \frac{\psi_n x \psi(\chi)}{\epsilon_e} \right\rangle + \left\langle \frac{\psi_n \psi'(\chi)}{\epsilon_e} \right\rangle \pm \frac{\beta_\mu(\chi)}{\beta_{|n|}} \left\langle \frac{\psi_n \psi'(\chi)}{\epsilon_e} \right\rangle \pm j \frac{\beta_\mu^2(\chi)}{\beta_{|n|}} \left\langle \frac{\psi_n x \psi(\chi)}{\epsilon_e} \right\rangle \pm j \frac{1}{\beta_{|n|}} \left\langle \frac{\psi_n \partial_x \psi(\chi)}{\epsilon_e} \right\rangle \right]. \tag{A21b}$$

Two equations similar to (A19a) and (A19b) can be achieved by multiplying (A15) and (A17) by $\psi(\sigma)/\epsilon_e(x)$ and integrating, using again the orthonormality properties (A18); hence by adding and subtracting, the integrodifferential equation for the amplitude of the continuous spectrum is obtained:

$$C_m'(\sigma) + jR\beta_m(\sigma) C_m(\sigma) = \sum_{\nu=-N}^{N} S_{\nu m}'(\sigma) C_\nu + \sum_{\mu=\pm} \int_0^\infty S_\mu(\sigma, \chi) C_\mu(\chi)\, d\chi \tag{A22}$$

where $m = \pm$ and

$$S_{\nu m}'(\sigma) = -\frac{1}{2}\left[\left\langle \frac{\psi(\sigma)\psi_\nu'}{\epsilon_e} \right\rangle + j\beta_\nu \left\langle \frac{\psi(\sigma) x \psi_\nu}{\epsilon_e} \right\rangle \pm \frac{\beta_\nu}{\beta(\sigma)} \left\langle \frac{\psi(\sigma)\psi_\nu'}{\epsilon_e} \right\rangle \pm J \frac{\beta_\nu^2}{\beta(\sigma)} \left\langle \frac{\psi(\sigma) x \psi_\nu}{\epsilon_e} \right\rangle \pm j \frac{1}{\beta(\sigma)} \left\langle \frac{\psi(\sigma)\partial_x \psi_\nu}{\epsilon_e} \right\rangle \right] \tag{A23a}$$

$$S_\mu(\sigma, \chi) = -\frac{1}{2}\left[j\beta_\mu(\chi) \left\langle \frac{\psi(\sigma) x \psi(\chi)}{\epsilon_e} \right\rangle + \left\langle \frac{\psi(\sigma)\psi'(\chi)}{\epsilon_e} \right\rangle \pm \frac{\beta_\mu'(\sigma)}{\beta(\sigma)} (\chi = \sigma) \pm \frac{\beta_\mu(\chi)}{\beta(\sigma)} \left\langle \frac{\psi(\sigma)\psi'(\chi)}{\epsilon_e} \right\rangle \pm j \frac{\beta^2(\chi)}{\beta(\sigma)} \left\langle \frac{\psi(\sigma) x \psi(\chi)}{\epsilon_e} \right\rangle \pm \frac{1}{\beta(\sigma)} \left\langle \frac{\psi(\sigma)\partial_x \psi(\chi)}{\epsilon_e} \right\rangle \right]. \tag{A23b}$$

Appendix III

By evaluating the integral over ζ in (19) we obtain

$$b_n = \sum_{m=1}^{n} \left[a_m (I_{n-m} - I_{n+1-m}) + b_m \Delta\phi\, I_{n-m} + b_m (J_{n-m} - J_{n+1-m}) \right] \tag{A24}$$

where

$$I_m = \int_0^\infty \frac{e^{j[\beta_1 - \beta(\chi)] R m \Delta\phi}}{-j[\beta_1 - \beta(\chi)] R} S_1^o(\chi) S_1'^o(\chi)\, d\chi \tag{A25a}$$

$$J_m = \int_0^\infty \frac{e^{j[\beta_1 - \beta(\chi)] R m \Delta\phi}}{[\beta_1 - \beta(\chi)]^2 R^2} S_1^o(\chi) S_1'^o(\chi)\, d\chi. \tag{A25b}$$

Recalling that

$$a_m + b_m \Delta\phi = a_{m+1} \tag{A26}$$

(A24) can be expressed as

$$b_n = a_n I_0 - a_1 I_n + b_n \Delta\phi : I_0 + \sum_{m=1}^{n} b_m (J_{n-m} - J_{n-m+1}) \tag{A27}$$

which becomes

$$b_n [1 - \Delta\phi\, I_0 - (J_0 - J_1)] = a_n I_0 - a_1 I_n + \sum_{m=1}^{n-1} b_m (J_{n-m} - J_{n+1-m}) \tag{A28}$$

leading to (20).

Integrations (A25) cannot be performed merely by numerical techniques, owing to an integrable singularity in $S_1'^o(\chi)$ and because the exponential term can be a rapidly oscillating function; on the other hand, asymptotic evaluation, with the method of say, stationary phase, gives inaccurate results.

However, operating a change of variable

$$\chi = n_2 k_0 \sin\theta \tag{A29a}$$

$$\beta(\chi) = n_2 k_0 \cos\theta \tag{A29b}$$

the singularity in $S_1'^o(\chi)$ is removed and, restricting integration to propagating waves only, the domain becomes

$0 \leqslant \theta \leqslant \pi/2$. This truncation does not affect in practice the values of the integrals because the integrand involving the evanescent components of the continuous spectrum is several orders of magnitude smaller than that involving the propagating components.

Subdividing the interval of integration into L subintervals ($\Delta\theta = \pi/2L$), equations (A25) can be written as

$$I_m(J_m) = \sum_{l=1}^{L} \int_{(l-1)\Delta\theta}^{l\Delta\theta} e^{j(\beta_1 - n_2 k_0 \cos\theta) R m \Delta\phi} f^{I(J)}(\theta)\, d\theta \tag{A30}$$

where

$$f^I(\theta) = \frac{S_1^o(\theta) S_1'^o(\theta) n_2 k_0 \cos\theta}{-j^{[\beta_1 - n_2 k_0 \cos\theta] R}} \tag{A31a}$$

$$f^J(\theta) = \frac{S_1^o(\theta) S_1'^o(\theta) n_2 k_0 \cos\theta}{[\beta_1 - n_2 k_0 \cos\theta]^2 R^2}. \tag{A31b}$$

If in each subinterval $(l-1)\Delta\theta \leqslant \theta \leqslant l\Delta\theta$, we assume a linearization of (A31a) and (A31b),

$$f^{I(J)}(\theta) \simeq A_l^{I(J)} \sin\theta + B_l^{I(J)} \sin\theta\cos\theta \tag{A32}$$

with constants A_l, B_l, the integral (A30) can then be easily evaluated in a closed form. The value of L is chosen so as to obtain the best fit in (A32).

References

[1] W. V. McLevige, T. Itoh, and R. Mittra, "New waveguide structures for millimeter-wave and optical integrated circuits", *IEEE Trans. Microwave Theory Tech.*, vol. MTT-23, pp. 788–794, Oct. 1975.

[2] T. Rozzi, T. Itoh, and Grün, "Two dimensional analysis of the GaAs d.h. stripe geometry laser," *Radio Sci.*, vol. 12, no. 4, July–Aug., pp. 543–549, 1977.

[3] J. Kot and T. E. Rozzi, "Rigorous modelling of single and coupled rectangular dielectric waveguide by transverse resonance diffraction," in *Proc. XIV European Microwave Conf.* (Liege), Sept. 10–13, 1984, pp. 424–429.

[4] M. Koshiba and M. Suzuki, "Vectorial wave analysis of dielectric waveguides for optical integrated circuits using equivalent network approach," *J. Lightwave Technol.*, vol. LT-4, pp. 656–664, June 1986.

[5] E. A. J. Marcatili, "Bends in optical dielectric guides," *Bell Syst. Tech. J.*, vol. 48, no. 7, pp. 2103–2133, Sept. 1969.

[6] D. Marcuse, "Bent optical waveguide with lossy jacket," *Bell Syst. Tech. J.*, vol. 53, pp. 1079–1101, July–Aug. 1974.

[7] D. Marcuse, *Light Transmission Optics* New York: Van Nostrand Reinhold, 1972.

[8] R. Baets and P. E. Lagasse, "Loss calculation and design of arbitrarily curved integrated-optic waveguides," *J. Opt. Soc. Amer.*, vol. 73, no. 2, pp. 177–182, Feb. 1983.

[9] V. V. Shevchenko, *Continuous Transition in Open Waveguides*. Boulder, CO. Golem Press, 1971.

[10] P. C. Kendall, P. N. Robson, and J. E. Sitch, "Rib waveguide curvature loss: The scalar problem," *Proc. Inst. Elec. Eng.*, vol. 132, pt. J, no. 2, pp. 140–145, Apr. 1985.

[11] M. W. Austin, "GaAs/GaAlAs curved rib waveguides," *IEEE J. Quantum Electron.*, vol. QE-18, pp. 795–800, Apr. 1982.

[12] K. Solbach, "The measurement of the radiation losses in dielectric image line bends and the calculation of a minimum acceptable curvature radius," *IEEE Trans. Microwave Theory Tech.*, vol. MTT-27, pp. 51–53, Jan. 1979.

[13] T. Yoneyama, H. Tamaky, and S. Nishida, "Analysis and measurements of non-radiative dielectric waveguide bends," *IEEE Trans. Microwave Theory Tech.*, vol. MTT-34, pp. 876–882, Aug. 1986.

[14] T. E. Rozzi, "Rigorous analysis of the step discontinuity in a planar dielectric waveguide," *IEEE Trans. Microwave Theory Tech.*, vol. MTT-26, pp. 738–746, Oct. 1978.

[15] T. E. Rozzi, and G. H. Int'Veld, "Field and network analysis of interacting step discontinuities in planar dielectric waveguides," *IEEE Trans. Microwave Theory Tech.*, vol. MTT-27, pp. 303–309, Apr. 1979.

[16] S. F. Mahmoud and J. C. Beal, "Scattering of surface waves at a dielectric discontinuity on a planar wavegude," *IEEE Trans. Microwave Theory Tech.*, vol. MTT-23, pp. 193–198, Feb. 1975.

[17] T. Rozzi, F. Cheung, and G. Cerri, "Cross-polarisation coupling in curved dielectric ridge waveguides," to be published.

T. Rozzi (M'66–M'74) obtained the degree of 'Dottore' in physics from the University of Pisa in 1965 and the Ph.D. degree in electronic engineering at Leeds University in 1968. In June 1987 he received the degree of D.Sc from the University of Bath.

From 1968 to 1978 he was a Research Scientist at the Philips Research Laboratories, Eindhoven, the Netherlands, having spent one year, 1975, at the Antenna Laboratory, University of Illinois, Urbana. In 1975 he was awarded the Microwave Prize of the Microwave Theory and Technique Group of the Institute of Electrical and Electronic Engineers. In 1978 he was appointed to the Chair of Eelctrical Engineering at the University of Liverpool and subsequently was appointed to the Chair of Electronics and Head of the Electronics Group at the University of Bath in 1981. From 1983 to 1986 he held the additional responsibility of Head of the School of Electrical Engineering at Bath. Since 1986 Dr. Rozzi has also held the 'ordinary chair' of Antennas at the Faculty of Engineering, University of Ancona, Italy.

Graziano Cerri was born in Ancona, Italy, in 1956. He received the degree in electronic engineering from the University of Ancona in 1981.

Since 1983, after military service in Air Force Engineer Corps, he has been with the Department of Electronics and Automatics at the University of Ancona as a researcher. His research is mainly devoted to microstrip antennas and integrated optics. He is also involved in the development of a system for microwave hyperthermia.

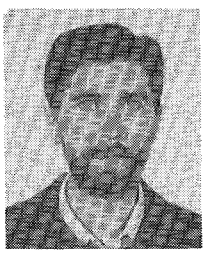

Franco Chiaraluce was born in Ancona, Italy, in 1960. He received the degree in electronic engineering from the University of Ancona in 1985. He is currently working in the Department of Electronics and Automatics at the University of Ancona. His research activities are primarily in the area of integrated optic device modeling.

Roberto De Leo was born in Bari, Italy, in 1942. He graduated from the Politecnico di Torino in 1965.

From 1966 to 1980 he was at the University of Bari, working on microwave devices. Since 1980 he has been a Full Professor of Electromagnetics at the University of Ancona. His area of interest concerns microwave hyperthermia and optoelectronic devices.

✠

Richard F. Ormondroyd received the B. Eng. and Ph.D. degrees in electronic and electrical engineering from the University of Sheffield in 1971 and 1975, respectively. His Ph.D. research topic was a study of

the electrical properties of amorphous chalcogenide glasses.

In 1975 he was appointed Lecturer in the School of Electrical Engineering, University of Bath, Bath, England, where his immediate research interests were the application of spread-spectrum techniques to communication systems. Since 1981 he has been involved in the development and fabrication of semiconductor lasers at the University of Bath. In 1985 he became Senior Lecturer and he is currently involved with work on multistripe lasers, optical bistability and switching, and active integrated optics.